Civil, Architectural and Environmental Engineering Faculty Research & Creative Works

Civil, Architectural and Environmental Engineering

26 Oct 2017

Seismic Performance of Hollow-Core Composite Columns under Cyclic Loading

Mohanad M. Abdulazeez

Mohamed ElGawady
Missouri University of Science and Technology, elgawadym@mst.edu

Recommended Citation

Seismic Performance of Hollow-Core Composite Columns under Cyclic Loading

Mohanad M. Abdulazeez[1], Mohamed A. ElGawady[2]

[1] *Graduate Research Assistance, Dept. of Civil, Architectural, and Environmental Engineering, Missouri University of Science and Technology, Rolla, MO. 65409*

[2] *Benavides Associate Professor, Dept. of Civil, Architectural, and Environmental Engineering, Missouri University of Science and Technology, Rolla, MO. 65409*

(mma548@mst.edu, elgawadym@mst.edu)

ABSTRACT

This paper experimentally investigates the seismic behavior of a large-scale, hollow-core, fiber-reinforced, polymer-concrete-steel HC-FCS column under cyclic loading. The typical precast HC-FCS member consists of a concrete wall sandwiched between an outer fiber-reinforced polymer (FRP) tube and an inner steel tube. The FRP tube provides continuous confinement for the concrete wall, along the height of the column. The column is inserted into the footing and temporarily supported; then, the footing is cast in place around the column. The seismic performance of the precast HC-FCS columns was assessed and compared with previous experimental work. The compared column had the same geometric properties; but the steel tube was 25% thicker than the column that was tested in this study. This paper revealed that these HC-FCS column assemblies were deemed satisfactory by developing the whole performance of such columns and using that performance to provide excellent ductility with inelastic deformation capacity by alleviating the damage at high lateral drifts.

Keywords: Seismic performance, Composite columns, Hollow core, Fiber Reinforced Polymer, Cyclic loading, Energy dissipation.

1. INTRODUCTION

The Federal National Bridge Inventory (FHWA 2013) classifies 63,522 bridges as "structurally deficient", 84,348 bridges as 'functionally obsolete" and many others as needing to be repaired, rehabilitated or replaced. Therefore, there is an urgent need for a rapid construction method to address this challenge.

Accelerating bridge construction (ABC) will reduce traffic disruptions and life-cycle costs as well as improve construction quality and safety, resulting in more sustainable development (Dawood et al. 2014). The use of precast concrete bridge elements is one strategy that can reduce on-site construction time, field labor requirements and traffic impacts. Precasting also improves the safety and quality of construction.

Recently, there has been a large and rapidly-growing interest in using fiber-reinforced polymer (FRP) tubes in construction as a replacement for the outer steel tube of the DSTCs column (Teng and Lam 2004; Teng et al. 2007). The proposed column is introduced as a hollow core FRP-Concrete-Steel (HC-FCS) column. The column consists of an inner steel tube and an outer FRP tube, with a concrete shell placed in between the two tubes (Fig. 1 (a)). FRP fibers are oriented in the hoop direction to increase the concrete confinement and provide more shear resistance (Zhang et al. 2012). HC-FCS composite columns as a precast element have several advantages over conventional reinforced concrete or structural steel that can be delivered from the combination of all three-component materials. The concrete infill is confined by both FRP and steel tubes, which results in a triaxial state of compression that increases the strength and strain capacity of the concrete infill and enhances the seismic performance of such columns (Abdelkarim and ElGawady 2014; Abdelkarim and ElGawady 2015; Abdelkarim and ElGawady 2016; Abdulazeez et al. 2017).

The main objective of this study is to investigate the performance of HC-FCS columns under axial and static dynamic loads in the hope of achieving a robust column under inelastic cyclic deformations that is of high-quality and easy to construct.

2. EXPERIMENTAL PROGRAM

In this study, a 0.4-scale HC-FCS column, F4-24-E3(1.5)4, with an embedment steel tube length of 635 mm corresponding to 1.6 D_i (D_i is the inner diameter of the steel tube) was tested under a constant axial load and a lateral cyclic load. The F4-24-E3(1.5)4 column had a circular cross-section with an outer

diameter of 610 mm and a clear height of 2,032 mm. The lateral load was applied at a height of 2,413 mm with a shear span-to-depth ratio of approximately 4.0. The column consisted of an outer filament-wound GFRP tube with a constant thickness of 9.5 mm, along the height of the column. The inner steel tube had an outer diameter of 406 mm and a thickness of 4.8 mm. A concrete wall with a thickness of 102 mm was sandwiched between the steel and FRP tubes (Fig. 1 (a)).

The columns' label used in the current experimental work consists of four segments. The first segment is a letter F referring to the flexural testing followed by the column's height-to-outer diameter ratio (H/D_o). The second segment refers to the column's outer diameter (D_o) in inches. The third segment refers to the GFRP matrix using E for epoxy base matrices; this is followed by a GFRP thickness of 1/8 inch (3.2 mm), steel thickness of 1/8 inch (3.2 mm) and concrete wall thickness of one inch (25.4 mm).

The concrete footing that was used in this study was 1,524 mm long x 1,220 mm wide x 864 mm deep with bottom reinforcements of 7-#7, top reinforcements of 6-#7 and a shear reinforcement of #4 @ 64 mm (Fig. 1). The steel cage of the footing was installed into the formwork. The construction steps are: (1) preparing and installing the reinforcement cages of the footings, (2) installing the steel tube inside the footing cage with an embedded length of 635 mm, (3) pouring the concrete of the footing (Fig. 2 (a)), (4) installing the GFRP tube and pouring the concrete of the column (Fig. 2 (b)) and (5) installing the reinforcement cage of the column head and concrete pouring to finally get the HC-FCS column (Fig. 2 (c)). The mechanical properties of the steel tube and rebar are summarized in Table 1. The rebar properties are based on the manufacturer's data sheet, while the steel tube properties were determined through tensile steel-coupon testing according to ASTM A 1067. The concrete mix design is shown in Table 2. Pea gravel with a maximum aggregate size of 9.5 mm was used for the concrete mixtures. Table 3 summarizes the unconfined concrete strength for the footings and columns. The material properties of the glass FRP tubes are presented in Table 4.
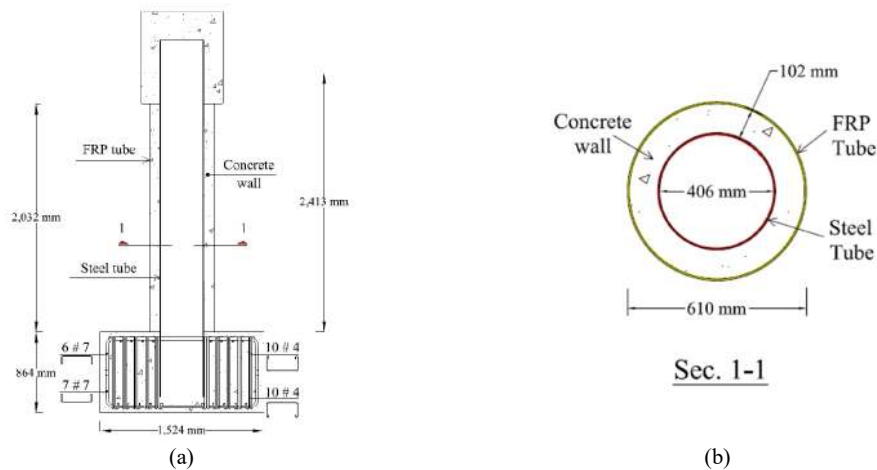

Fig. 1. Construction layout of the column (a) Elevation, (b) column cross-section

Fig. 2. Constructing procedure (a) footing casting around the inner steel tube; (b) placing the FRP tube and pouring the concret wall; (c) the HC-FCS column

Table 1. Steel properties of the rebars and steel tube

	Elastic modulus (E, GPa)	Yield stress (f_y, MPa)	Ultimate stress (f_u, MPa)	Ultimate strain (ε_u, mm/mm)
Steel rebar	200	413.7	620.5	0.08
Steel tube	200	399	441	0.22

Table 2. Concrete mixture proportions

w/c	Cement (kg/m^3)	Fly Ash (kg/m^3)	Water (kg/m^3)	Fine Aggregate (kg/m^3)	Coarse Aggregate (kg/m^3)
0.5	350	101	225	848	848

Table 3. Summary of the unconfined concrete strength of the columns and the footings

	F4-24-E3(1.5)4		F4-24-P324	
	Column	Footing	Column	Footing
f'_c at 28 days (MPa)	35	55	32.6	36.6
f'_c day of test (MPa)	46.5	56.7	36	39

Table 4. FRP tubes properties

Elastic modulus (GPa)	Hoop elastic Modulus (GPa)	Axial ultimate stress (MPa)	Hoop rupture stress (MPa)
4.7	21	83.8	276.8

2.1. Experimental set-up and instrumentations

Sixteen Linear-Variable-Displacement-Transducers (LVDTs) and String Potentiometers (SPs) were assigned for measuring displacement along the tested column F4-24-E3(1.5)4. A layout of the LVDTs and SPs is shown in (Fig. 3 (a)). Four LVDTs were mounted on each of the north and south faces for the vertical displacement measurements at the potential plastic hinge region. Two more LVDTs were attached for measuring the uplift and sliding of the footing during the test. The effect of the footing uplift and sliding were considered before calculating the lateral displacement and curvature of the column.

(a)   (b)   (c)
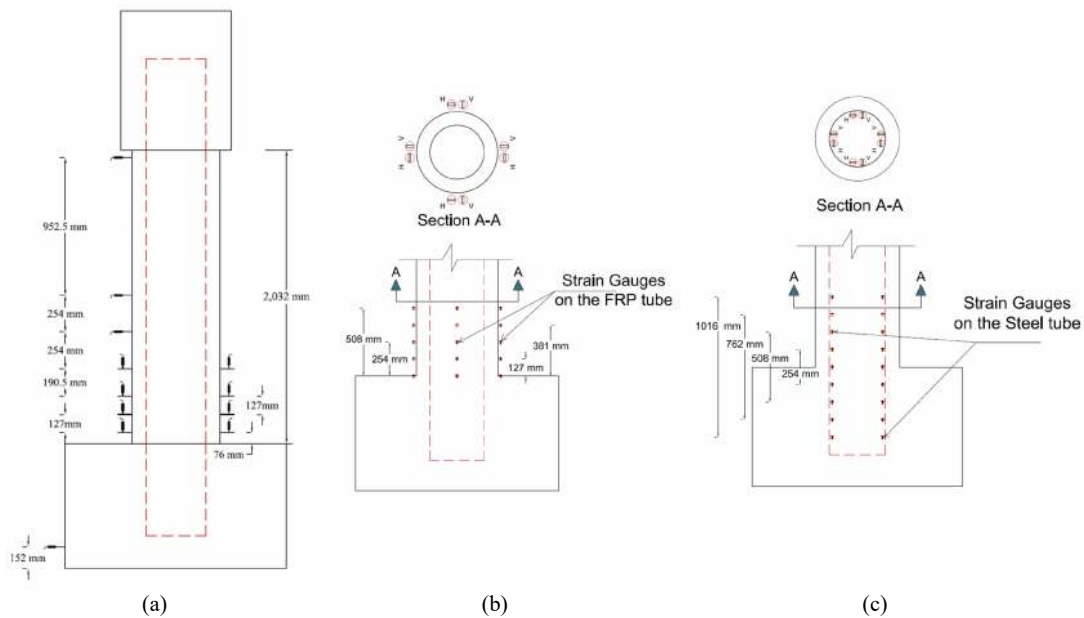
Fig. 3. Straing gauges layout: (a) LVDT's and SP's installing; (b) mounted on GFRP tube; and (c) mounted on Steel tube

Forty strain gauges were installed on the FRP tube at five levels with 127 mm of space between them. Four horizontal and four vertical strain gauges were installed at each level as shown in (Fig. 3 (b)). Seventy-two strain gauges were installed inside the steel tube at seven levels with a spacing of 127 mm (Fig. 3 (c)). Four horizontal and four vertical strain gauges were installed at each level here as well. A high-definition webcam was hung vertically inside the steel tube at 635 mm from the top of the footing level.

2.2. Loading protocol and test setup

The constant axial load, P, of 489.3 kN corresponds to 5% of the axial load capacity of the equivalent RC-column, P_o, and has the same diameter. A 1% longitudinal reinforcement ratio was applied to the column using six external prestressing strands (Fig. 4 (a)). The P_o was calculated using Eqn. 1 (AASHTO-LRFD 2012):

$$P_a = A_s F_y + 0.85 (A_c - A_s) f'c \qquad (1)$$

where A_s = the cross-sectional area of the longitudinal steel reinforcements, A_c = the cross sectional area of the concrete column, F_y = the yield stress of the longitudinal steel reinforcements, and $f'c$ = the cylindrical concrete's unconfined compressive stress. The prestressing strands were supported by a rigid steel beam atop the column and the column's footing. The prestressing force was applied using two servo-controlled jacks to keep the prestressing force constant during the test.
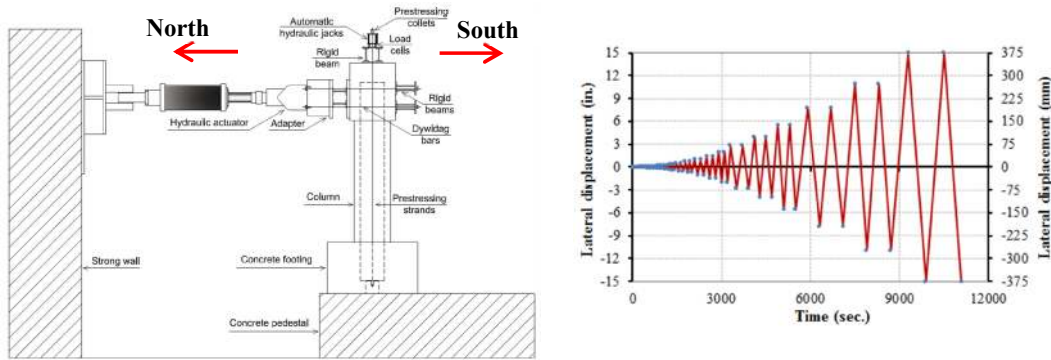

Fig. 4. (a) Layout of the test setup; (b) Lateral displacement loading regime

After applying the axial load, the cyclic lateral load was applied in a displacement control using two hydraulic actuators connected to the column loading stub. The loading regime is based on the recommendations of FEMA in 2007 where the displacement amplitude a_{i+1} of the step i+1 is 1.4 times the displacement amplitude of the proceeding step (a_i). Two cycles were executed for each displacement amplitude. Figure 4 (b) illustrates the loading regime of the cyclic lateral displacement. Each loading cycle was applied in 100 sec., corresponding to a loading rate which ranged from 0.254 mm/sec. to 1.27 mm/sec.

3. RESULTS AND DISCUSSIONS

The moment-lateral drift plot is shown in (Fig. 5 (a)). The lateral drift (δ) was calculated by dividing the lateral displacement, which was measured from the actuators' displacement transducers by the shear span of 2,413 mm. The moment (M) at the base of the column was obtained by multiplying the force measured by the actuators' loading cells by the column's height of 2,413 mm. Figure 5 (a) and Table 5 illustrate the comparison between the cyclic response of the two columns F4-24-E324 and F4-24-E3(1.5)4. As shown in the figure and the table, column F4-24-E3(1.5)4 displayed 7% less flexural strength at 680 kN.m and 35% less maximum lateral drift at 8.4% compared to column F4-24-E324. Gradual stiffness degradation occurred beyond that until the end of the test. The stiffness degradation

occurred because of the concrete damage inside the tube. The buckling of the steel tube led to the initiation of ductile tearing at 8.0% of the column-footing interface area and, thereby, the end of the test.

Table 5. Result Summary of the two tested columns

Tested Column	Moment capacity (kN.m)	Lateral drift at max. moment (%)	Lateral drift at failure (%)	Mode of failure
F4-24-E3(1.5)4	680.0	2.7	8.4	Steel tube local buckling, concrete crushing, and steel tube ductile tearing
F4-24-E324 (Abdelkarim et al. 2015)	732.0	2.8	13.0	Steel tube local buckling, concrete crushing, and FRP tube rupture

For the investigated columns, the energy dissipation at each lateral drift was determined by the area enclosed in the hysteretic loop of the first cycle at this drift level. Dissipating higher hysteretic energy reduces the seismic demand on a structure. Figure 5 (b) illustrates the relationship between the cumulative energy dissipation and the lateral drift for columns F4-24-E3(1.5)4 and F4-24-E324 that have been tested by Abdelkarim et al. (2015). As shown in the figure, both columns dissipated the same level of energy until a drift of approximately 2.5% was reached. Beyond that, column F4-24-E3(1.5)4 dissipated a much smaller amount of energy due to the severe local buckling followed by the ductile tearing of the steel tube. At a drift of 8.4% when column F4-24-E3(1.5)4 failed, column F4-24-E324 dissipated 240% more energy.
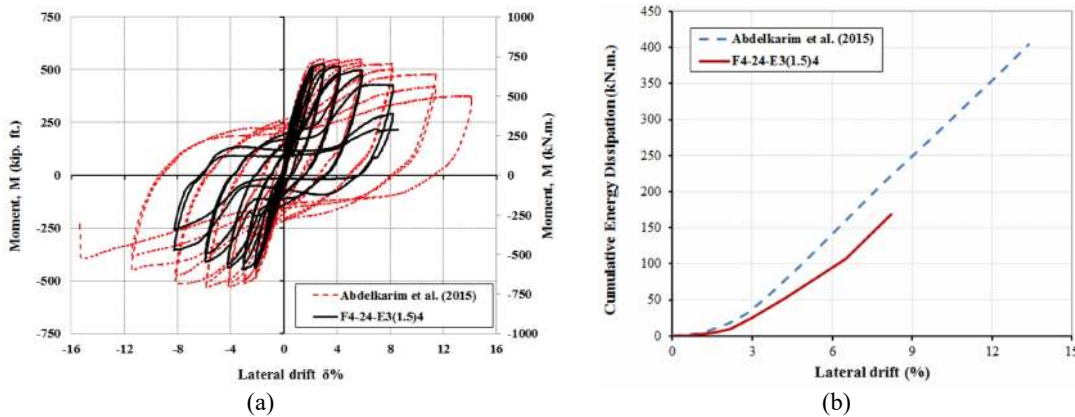

Fig. 5. Moment vs. lateral drift for columns F4-24-E3(1.5)4 and F4-24-E324 (Abdelkarim et al. 2015), (b) Cumulative energy dissipation vs. lateral drift for columns F4-24 E3(1.5)4 and F4-24-E324 (Abdelkarim et al. 2015)

4. CONCLUSIONS

This paper presents the experimental results of a hollow-core, fiber-reinforced, polymer-concrete steel (HC-FCS) precast column. The HC-FCS column consists of a concrete hollow cylinder sandwiched between an outer fiber-reinforced polymer (FRP) tube and an inner steel tube. The column had an outer diameter of 610 mm, an inner steel tube diameter of 406 mm and a height-to-diameter ratio of 4.0. The steel tube was embedded into reinforced concrete footing with an embedded length of 1.6 times the steel tube's diameter, while the FRP tube acted as a formwork, provided a continuous confinement for the concrete wall and was curtailed at the top surface of the footing. The column was subjected to constant a axial load and lateral cyclic load during this study and compared to the HC-FCS column that was tested by Abdelkarim et al. (2015) under the same loading regime. The HC-FCS F4-24-E3(1.5)4 column failed at a drift of 8.4% due to the concrete wall crashing and the steel tube buckling, followed by ductile tearing at the column-footing interface level.

ACKNOWLEDGEMENT

REFERENCES

Abdelkarim, O. I., and ElGawady, M. A. (2014). "Analytical and Finite-Element Modeling of FRP-Concrete-Steel Double-Skin Tubular Columns." *Journal of Bridge Engineering*.

Abdelkarim, O. I., and ElGawady, M. A. (2015). "Concrete-Filled-Large Deformable FRP Tubular Columns under Axial Compressive Loading." *Fibers*, 3(4), 432-449.

Abdelkarim, O. I., and ElGawady, M. A. (2016). "Behavior of hollow FRP–concrete–steel columns under static cyclic axial compressive loading." *Engineering Structures*, 123, 77-88.

Abdelkarim, O. I., Gheni, A., Anumolu, S., and ElGawady, M. A. "Seismic behavior of hollow-core FRP-concrete-steel bridge columns." *Proc., Structures Congress 2015*, 585-596.

Abdelkarim, O. I., Gheni, A., Anumolu, S., Wang, S., and ElGawady, M. (2015). "Hollow-Core FRP-Concrete-Steel Bridge Columns Under Extreme Loading."

Abdulazeez, M. M., Abdelkarim, O. I., Gheni, A., ElGawady, M. A., and Sanders, G. (2017). "Effects of Footing Connections of Precast Hollow-Core Composite Columns."

Dawood, H., Elgawady, M., and Hewes, J. (2014). "Factors affecting the seismic behavior of segmental precast bridge columns." *Frontiers of Structural and Civil Engineering*, 8(4), 388-398.

Teng, J., and Lam, L. (2004). "Behavior and modeling of fiber reinforced polymer-confined concrete." *Journal of structural engineering*, 130(11), 1713-1723.

Teng, J., Yu, T., Wong, Y., and Dong, S. (2007). "Hybrid FRP–concrete–steel tubular columns: concept and behavior." *Construction and Building Materials*, 21(4), 846-854.

Zhang, B., Teng, J., and Yu, T. (2012). "Behaviour of hybrid double-skin tubular columns subjected to combined axial compression and cyclic lateral loading."